

Luminescence decay dynamics of germanium nanocrystals in silicon

B. Julsgaard,^{1, a)} P. Balling,¹ J. Lundsgaard Hansen,¹ A. Svane,¹ and A. Nylandsted Larsen¹

Department of Physics and Astronomy, Aarhus University, DK-8000 Aarhus C, Denmark

(Dated: 9 October 2018)

The dynamics of the luminescence decay from germanium nanocrystals embedded in crystalline silicon has been studied for temperatures varied between 16 K and room temperature. At room temperature the characteristic decay time is of the order of 50 nanoseconds while it extends into the microsecond range at low temperatures. The decay is dominated by non-radiative processes, which show a typical thermal activation energy of a few meV.

Luminescence from germanium (Ge) nanocrystals embedded in silicon (Si) is interesting since the emission wavelength can be tuned in the range around $1.5\mu\text{m}$ used by standard fiber communication technology. Hence such nanocrystals present one of several routes toward integration of optical and electronic functionality on a silicon chip. Previously, the spectral dependence of the luminescence from Ge (or SiGe) nanocrystals has been studied as a function of various growth parameters,¹⁻⁷ and experimental parameters^{6,8,9} such as sample temperature, laser excitation power and wavelength, and stress, often in search of a deeper understanding of the Ge/Si system (e.g. band edge alignment¹⁰). Some of these studies have demonstrated room-temperature luminescence,^{1,2,4,7} but luminescence life time measurements have only been presented to a very limited extent.^{2,8}

In this letter we study the dynamics and spectral characteristics of the luminescence from Ge nanocrystals as a function of temperature from room temperature down to 16 K. By lowering the temperature, a significant increase in the decay time is observed as the most pronounced effect, leading to our conclusion that the decay is dominated by non-radiative processes. In addition, the decay behavior can be interpreted consistently with models of Ge/Si nanocrystals published previously.^{6,10}

Self-assembled Stranski-Krastanow Ge nanocrystals were prepared by molecular beam epitaxy. On a Si(100) wafer ($\approx 100\ \Omega\text{cm}$) a 200 nm Si buffer layer was grown

followed by a layer of Ge, which was deposited without rotating the wafer leading to a non-uniform Ge layer thickness. Finally, a 50 nm Si capping layer was added. A surfactant⁷ of approximately 0.01 mono-layer of antimony (Sb) was used, and the growth temperature was 530 °C. Five pieces with nominal Ge layer thicknesses of 8.25, 9.00, 9.75, 10.50, and 11.50 Å have been cut from the wafer. A transmission electron micrograph (TEM) obtained for the sample with nominal Ge-layer thickness of 9.75 Å shows that nanocrystals have been formed with diameters around 20 nm, see Fig. 1.

The samples were mounted in a closed-cycle helium cryostat allowing for sample temperatures down to 16 K. An amplified 1 kHz femto-second Ti:sapphire laser system was frequency doubled in order to produce 100 fs pulses at 400 nm (3.1 eV) for exciting the Ge nanocrystals. The laser pulse energy entering the sample was typically $6\ \mu\text{J}$, focused by a cylindrical lens with 100 mm focal length leading to a fluence of the order of $6 \cdot 10^{-4}\ \text{J}/\text{cm}^2$. The nanocrystal fluorescence was collected into a McPherson 218 spectrometer equipped with a liquid-nitrogen-cooled photo-multiplier tube (Hamamatsu R5509-73).

Time-resolved emission spectra obtained at room temperature are shown in Fig. 2(a,b). The spectra can be fitted reasonably to a sum of two Gaussian functions allowing an easy determination of the general trend of the emission characteristics. The peak just below 1.1 eV arises from band-edge recombination in bulk silicon. The lower-energy peak is only present in samples containing Ge, and its position changes toward lower energies during the first few tens of ns (compare panels a and b in Fig. 2). Decreasing the Ge-layer thickness leads to an increase of the emission energy for both the early-time and late-time peaks (Fig. 2c). This blue-shift in emission energy together with the requirement that Ge must be present indicates that the light is emitted from quantum confined Ge-related structures. Although emission from the Ge wetting layer (WL) is usually not observed in steady-state photo-luminescence experiments for samples grown at 530 °C, at least the emission energy of the early-time peak is in the correct range⁶. We attribute the late-time peak to emission from Ge nanocrystal islands in agreement with previous observations.¹⁻⁸ As can be seen in Fig. 2d, the sample with a nominal Ge-layer thickness

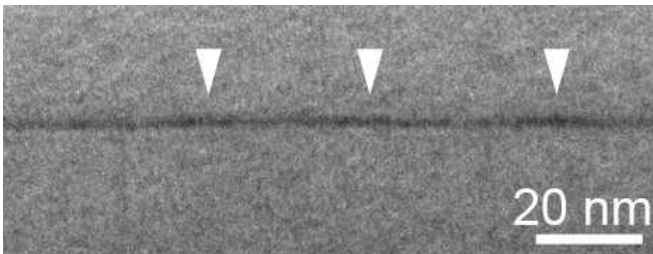


FIG. 1. Cross-sectional transmission electron micrograph showing that the Ge nanocrystals are barely rising above the wetting layer and the lateral size is of the order of 20 nm.

^{a)} Electronic mail: brianj@phys.au.dk.

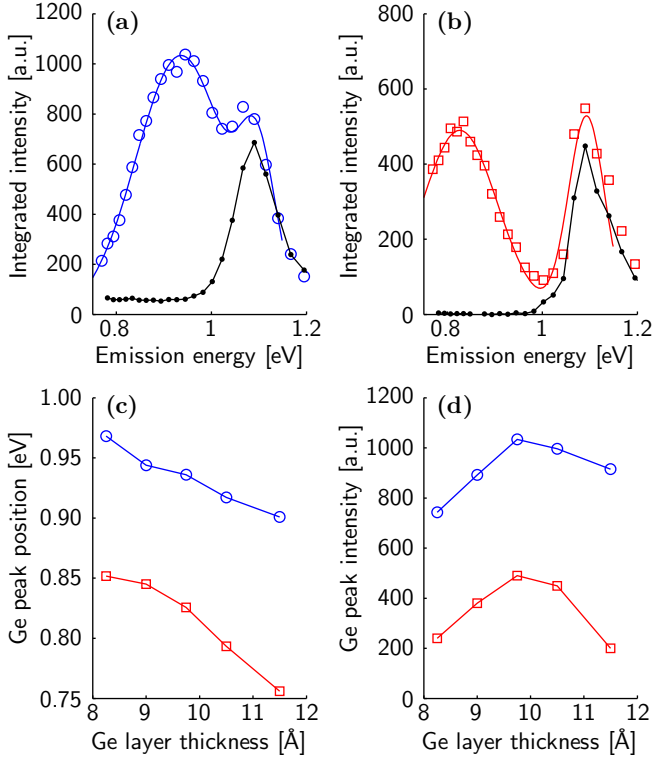


FIG. 2. (Color on-line) Panels a and b show time-resolved emission spectra of the sample with nominal Ge thickness of 9.75 Å at 294 K. The time range of the spectra are $0 \leq t \leq 5$ ns (blue circles) and $25 \text{ ns} \leq t \leq 200$ ns (red squares) for panels a and b, respectively. The data can be modeled approximately by a sum of two Gaussian peaks (solid lines). Spectra from a sample without Ge are shown for comparison (black dots). Panels c and d show (with symbols corresponding to those of panels a and b) the fitted position and height, respectively, of the lower-energy peak in the two-Gaussian model for various Ge layer thicknesses.

of 9.75 Å emits most light and we selected this sample for further investigations at varying temperature.

The separation of time scales into an early-time part (≈ 10 ns time scale) and a late-time part is evident when considering the luminescence decay curves shown in Fig. 3a. This graph shows decay curves obtained at the emission energy of 0.775 eV for varying temperatures. The initial peak is essentially independent on temperature, while the longer-time decay changes significantly with temperature. To clarify this effect further, we obtained time-resolved emission spectra in the time range, $0 \leq t \leq 5$ ns, which selects primarily the initial peak. The results have been plotted in Fig. 3b, and the similarity for varying temperature is evident. This challenges the interpretation that this light originates from WL emission: The insensitivity to temperature - i.e. the fact that the spectral feature remains broad - must be clarified in a more systematic study before a clear identification can be made. On the contrary, when setting the time range to $25 \text{ ns} \leq t \leq 200$ ns, and thereby selecting the late-

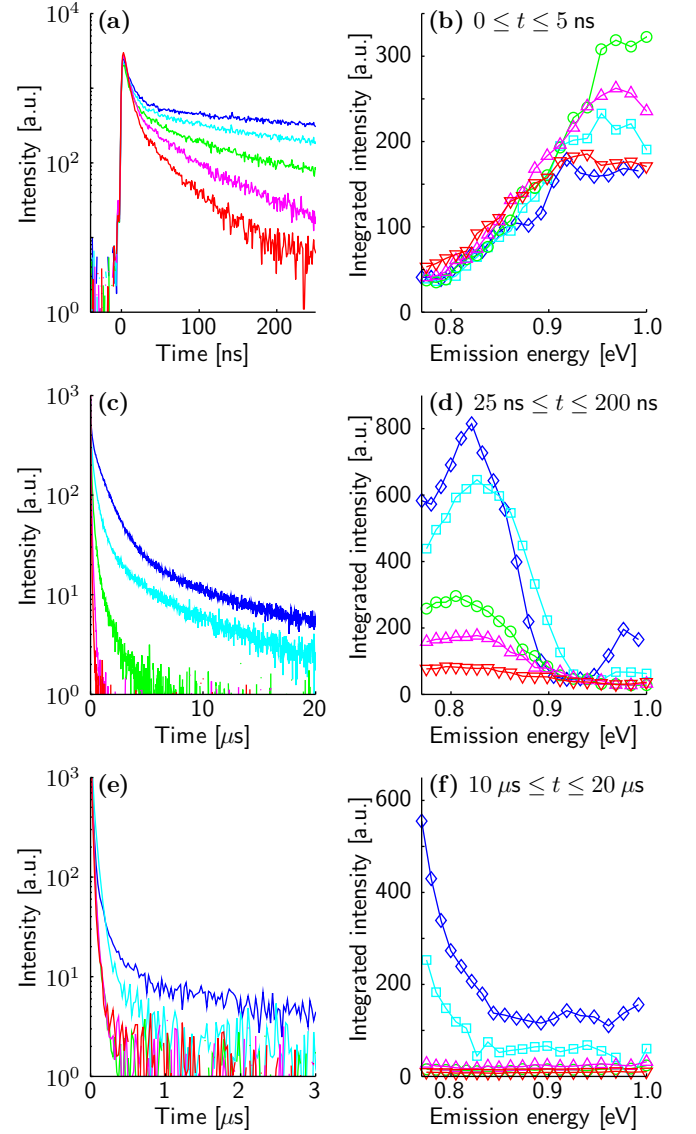


FIG. 3. (Color on-line) Decay curves (panels a, c, e) and time-resolved emission spectra (panels b, d, f) plotted for various temperatures: 294 K (red tip-down triangles), 200 K (purple tip-up triangles), 100 K (green circles), 40 K (cyan squares), and 22 K (blue diamonds). In panels (a, c, e) the upper graph shows the 22 K data, while the temperature increases through the above-mentioned values for the subsequent lower curves. The emission energy is 0.775 eV for the curves in panels a and c, and 0.886 eV in panel e. Time ranges for the spectra in panels b, d, and f are mentioned on the graphs.

time part of Fig. 3a, the emission characteristics of Ge islands are recovered as shown in Fig. 3d. The decrease in intensity with increasing temperature corresponds to observations reported previously.⁶

In order to investigate further the Ge island emission, we plot decay curves for longer time scales in Fig. 3c (0.775 eV) and Fig. 3e (0.886 eV). These curves show several features: (i) The decay time increases significantly when lowering the temperature, (ii) the low-energy side

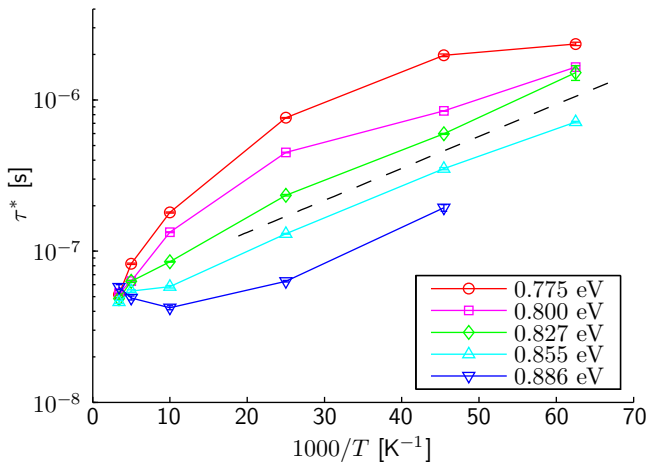


FIG. 4. (Color on-line) The characteristic decay time, τ^* , as a function of reciprocal temperature plotted for various emission energies. The error bars denote the statistical uncertainty from the fitting procedure. The dashed line corresponds to an activation energy of 4.2 meV.

of Ge island emission decays significantly slower than the high energy side, and (iii) there is an asymptotic limit for the decay curves; zooming in on the high-temperature curves in panels c and e of Fig. 3 would reveal essentially the same decay behavior. From these observations we suggest that two distinct decay mechanisms co-exist, where one is much more robust to high temperatures than the other.

We also note that for the lowest temperatures a distinct decay component with a very slow decay time arises. If the uppermost graph in Fig. 3c is fitted to a single-exponential function in the range, $10 \mu s \leq t \leq 20 \mu s$, a decay time of $13 \mu s$ is found, while in the range, $1 \mu s \leq t \leq 3 \mu s$, the same procedure yields $1.6 \mu s$. In order to reveal the spectral behavior of the very-long-time component, a time-resolved emission spectrum for the time range, $10 \mu s \leq t \leq 20 \mu s$, is shown in Fig. 3f. We see that there is both a flat background above 0.85 eV and an increased intensity at lower energies. The latter suggests that the very-long-time emission originates at least partly from the Ge islands with a down-shifted emission energy (by 50 meV or more, compare Figs. 3d and f). Assigning the $\geq 10\text{-}\mu s$ component to spatially indirect transitions across the Ge/Si boundary and the $\approx 1\text{-}\mu s$ component to spatially direct transitions within the Ge nanocrystal would be consistent with previous results.⁶

In order to make a general comparison of the decay dynamics for various temperatures and emission energies, we make a multi-exponential fit to each decay curve modeled as: $f(t) = d_0 + \sum_{j=1}^N A_j \exp(-t/\tau_j)$. Here d_0 is the dark count level, and the number of terms, N , is adjusted in order to fit the entire decay curve reasonably (in practice N varies between 2 and 4). The fastest term will model the initial peak in Fig. 3a, which has a spectral characteristic (Fig. 3b) different from that of Ge

islands. In practice the fastest timescale varies between 6 ns and 12 ns within the temperatures and emission energies studied here. In the following analysis we exclude this fastest term in order to model more closely the actual Ge island emission. We define the characteristic decay time: $\tau^* = \text{Area}/\text{Amplitude} = (\sum_{j=2}^N A_j \tau_j) / (\sum_{j=2}^N A_j)$, where the “Area” (under the decay curve) is the integrated intensity and “Amplitude” is the initial intensity at zero time. Since τ^* is proportional to the integrated intensity, it represents in a direct way how an increased decay time leads to a more efficient light emission in total. In Fig. 4 we show Arrhenius plots of τ^* as a function of $1000/T$ for different emission energies. Most pronounced, when lowering the temperature the decay time becomes slower. The fact that τ^* increases significantly with decreasing temperature while the initial decay amplitude varies only modestly (extrapolating the late-time-part of the decay curves in Fig. 3a back to zero time will lead to roughly the same initial value) proves that the decay is dominated by non-radiative processes. Although the upper-most curve in Fig. 4 shows some effects of saturation, the general trend is a continued increase of τ^* for decreasing temperature and hence that non-radiative processes are dominant also at 16 K. We conclude that the radiative decay time must be at least well into the microsecond range. Such long radiative decay times are characteristic for indirect-band-gap materials.¹¹ We also note in Fig. 4 that the non-radiative decay processes are activated on the few-meV energy scale with little dependence on the emission energy (compare the data curves with the dashed line in Fig. 4). Assigning an energy barrier of this magnitude to a metastable electronic state within the Ge nanocrystal is consistent with the calculations of Ref.¹⁰ The lower bound around 50 ns is characteristic for the asymptotic decay curves discussed in relation to Fig. 3(c,e) and may arise, as discussed, from a separate emission mechanism.

In conclusion, we have measured the characteristic decay times for Ge nanocrystals as a function of emission energy and temperature. We demonstrate that the decay is dominated by non-radiative recombination mechanisms. A shallow few-meV energy barrier of electronic states within Ge nanocrystals is suggested as responsible for the non-radiative decay process.

This work was supported by The Danish Council for Independent Research | Natural Sciences and by the Carlsberg Foundation. We thank J. Chevallier for assistance with TEM measurements.

¹H. Sunamura, S. Fukatsu, N. Usami, and Y. Shiraki, *J. Cryst. Growth* **157**, 265 (1995).

²G. Bremond, M. Serpentine, A. Souifi, G. Guillot, B. Jacquier, M. Abdallah, I. Berbezier, and B. Joyced, *Microelectronics J.* **30**, 357 (1999).

³O. G. Schmidt, C. Lange, and K. Eberl, *Appl. Phys. Lett.* **75**, 1905 (1999).

⁴O. G. Schmidt, U. Denker, K. Eberl, O. Kienzle, and F. Ernst, *Appl. Phys. Lett.* **77**, 2509 (2000).

⁵M. W. Dashiell, U. Denker, and O. G. Schmidt, *Appl. Phys. Lett.* **79**, 2261 (2001).

- ⁶M. Larsson, A. Elfving, W.-X. Ni, G. V. Hansson, and P. O. Holtz, *Phys. Rev. B* **73**, 195319 (2006).
- ⁷A. Tonkikh, N. Zakharov, V. Talalaev, and P. Werner, *Phys. Stat. Sol. RRL* **4**, 224 (2010).
- ⁸S. Fukatsu, H. Sunamura, Y. Shiraki, and S. Komiyama, *Appl. Phys. Lett.* **71**, 258 (1997).
- ⁹B. Adnane, K. F. Karlsson, G. V. Hansson, P. O. Holtz, and W. Ni, *Appl. Phys. Lett.* **96**, 181107 (2010).
- ¹⁰M. El Kurdi, S. Sauvage, G. Fishman, and P. Boucaud, *Phys. Rev. B* **73**, 195327 (2006).
- ¹¹M. S. Hybertsen, *Phys. Rev. Lett.* **72**, 1514 (1994).